Fermi surface of $Hg_{3-\delta}AsF_6$ and $Hg_{3-\delta}SbF_6$

E. Batalla, F. S. Razavi, and W. R. Datars
Department of Physics, McMaster University, Hamilton, L8S 4M1 Canada

(Received 27 August 1981)

Measurements of the de Haas–van Alphen frequencies in $Hg_{3-\delta}AsF_6$ and $Hg_{3-\delta}SbF_6$ show that the Fermi surface of these compounds consists of cylinders with axes parallel to the c direction. A detailed model of the Fermi surface of these mercury linear-chain compounds is constructed for conduction electrons in the mercury chains. The cross-sectional areas of the Fermi-surface cylinders are accounted for by the Fermi-surface model. Cyclotron masses measured for some of the orbits are in satisfactory agreement with those predicted by the model. The excellent agreement between measured and predicted cross-sectional areas for both compounds shows that the model is valid for a range of values of the incommensurability parameter δ.

I. INTRODUCTION

$Hg_{3-\delta}AsF_6$ and $Hg_{3-\delta}SbF_6$ are compounds that contain one-dimensional chains of mercury atoms in two mutually perpendicular directions.[1] Their electrical[2,3] and optical[4,5] properties are anisotropic and metallic suggesting that the conduction electrons are localized in the channels containing the mercury chains. Reports of the de Haas–van Alphen effect (dHvA) in $Hg_{3-\delta}AsF_6$ (Ref. 6) and $Hg_{3-\delta}SbF_6$ (Ref. 7) show that they are two-dimensional conductors from coupled one-dimensional chains. The present paper is a full account of these experiments. Section II provides a short description of the crystal structure of these compounds. The results of the dHvA experiment are given in Sec. III. Our Fermi-surface model is presented in Sec. IV. A comparison of the data and the model is given in Sec. V.

II. CRYSTAL STRUCTURE

The crystal structure of the mercury linear-chain compounds $Hg_{3-\delta}AsF_6$ and $Hg_{3-\delta}SbF_6$ was determined at room temperature by Brown *et al.*[1] and Cutforth[8] using x-ray diffraction. They found that both compounds contain chains of mercury atoms in channels of a tetragonal lattice of octahedral anions. For $Hg_{3-\delta}AsF_6$ Pouget *et al.*[9] confirmed these results at room temperature and extended these measurements down to 10 K using neutron scattering. They found that the two mutually perpendicular sets of mercury chains order below 120 K.

At room temperature, the hexafluoride anions in $Hg_{3-\delta}AsF_6$ and $Hg_{3-\delta}SbF_6$ form a body-centered tetragonal lattice with a basis of two anions as shown in Fig. 1. An anion at the origin of the axes together with one at $(0, a/2, c/4)$ form the basis of the structure.

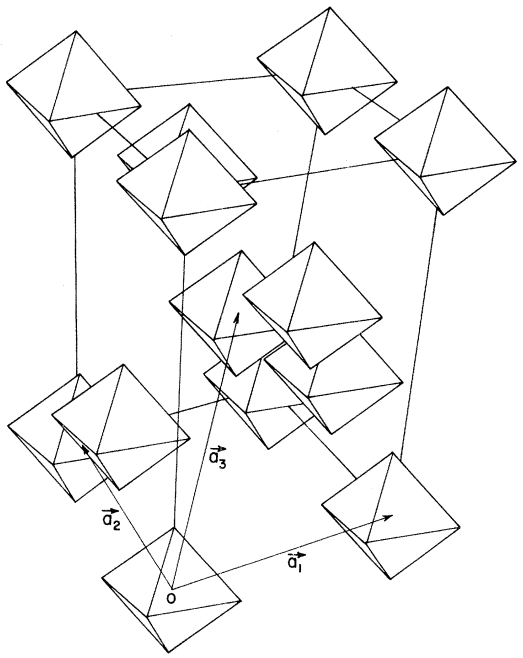

FIG. 1. Perspective view of the hexafluoride lattice of $Hg_{3-\delta}AsF_6$ with the unit cell represented by solid lines relative to primitive vectors $\vec{a}_1$, $\vec{a}_2$, and $\vec{a}_3$.

There are channels along the x and y axes of this structure intersecting the boundaries of the tetragonal unit cell in the yz and xz planes at $(0,0,\frac{3}{8})$, $(0,\frac{1}{2},\frac{7}{8})$, and at $(\frac{1}{2},0,\frac{1}{8})$, $(0,0,\frac{5}{8})$, respectively. These channels do not intersect because the channels along the x and y directions are a distance $c/4$ apart along the z direction. The mercury atoms are located in these channels and are arranged as shown in Fig. 2. Table I contains crystal structure parameters for $Hg_{3-\delta}AsF_6$ and $Hg_{3-\delta}SbF_6$.

The mercury-mercury distance along a channel direction d is not commensurate with the tetragonal lattice parameter a. The fact that less than three mercury atoms fit into the distance a is described by the incommensurability parameter δ such that $(3-\delta)d=a$. This gives the compound formulas $Hg_{3-\delta}AsF_6$ and $Hg_{3-\delta}SbF_6$. Also, sheets of diffuse x-ray scattering are observed establishing that there is no ordering of the position of Hg atoms in adjacent parallel chains at room temperature.

At 120 K, the mercury atoms in parallel chains are observed to order in $Hg_{3-\delta}AsF_6$.[9] Below 120 K if a mercury atom is at the origin of the x axis for a chain going in the x direction, then, on the parallel chain a distance a along the y axis, there is a mercury atom with a coordinate along the x-axis of $\pm\delta d$. In the chains that are one lattice parameter c from the two above, mercury atoms are at the same positions along the x axis while the atoms in the chains at $c/2$ are in body-center positions. If the sign of the displacement of the mercury atoms in going from a chain to the next parallel one is the same for both the chains along the x and y axes, the two structures have common reciprocal points of the form

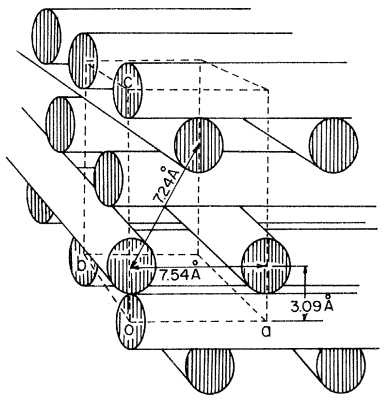

FIG. 2. Arrangement of the Hg chains in $Hg_{3-\delta}AsF_6$.

$$(h,k,l)=n(3-\delta,3-\delta,0)\ .$$

This means that there is some interaction between perpendicular chains. This is not unexpected since the distance of closest approach between perpendicular chains (3.085 Å at room temperature) is not very different from the mercury-mercury distance in metallic mercury (3.005 Å). Also, Pouget *et al.* report that the $(6-2\delta,\ 6-2\delta,0)$ peak is detected while the $(3-\delta,3-\delta,0)$ is not. They conclude from this that the phase of the two sets of chains is arranged such that the (110) planes containing the mercury atoms on the chains going in the x direction are exactly halfway between (110) planes containing the mercury atoms from the chains along the y axis.

III. de HAAS–van ALPHEN EFFECT

The dHvA effect was observed at 1.1 K in a magnetic field range 3–5.5 T. Single-crystal samples with approximate dimensions $2\times2\times1$ mm^3 contained in a sealed sample holder were mounted in a sensitive modulation-pickup-coil assembly. The holder, sealed when it was in a dry box, protected the sample from moisture which decomposes linear-chain mercury compounds very quickly. Samples could be turned about an axis perpendicular to the magnetic field direction to measure dHvA frequencies at fixed magnetic field directions in a (hk0) crystallographic plane.

The frequency of modulation was 517 Hz and the signal from the pick-up coil at the second harmonic of this frequency was detected. The field from a 5.5 T superconducting magnet was changed linearly in reciprocal field so that the dHvA oscillations were equally spaced in time. Fourier analysis of the signal amplitude recorded as a function of magnetic field on magnetic tape gave values of the dHvA frequencies.

The dHvA frequencies of $Hg_{3-\delta}AsF_6$ are shown in Fig. 3 as a function of the angle θ between the c axis and the magnetic field direction. The results consist of low-frequency branches α, β, and γ and high-frequency branches δ, ϵ, and μ. Branches α and γ disappear about $\theta=71°$ and β disappears at $\theta=60°$. The amplitudes of the β and γ frequencies are strong at all magnetic field directions while the amplitude of the α frequency is weak in all magnetic field directions, especially near the c axis. The δ and ϵ frequency branches disappear about $\theta=60°$ and the amplitude of δ is dominant in this frequency range. Branch μ disappears about 20°

TABLE I. Crystal-structure parameters and mercury-mercury distance along channels d for $Hg_{3-\delta}AsF_6$ and $Hg_{3-\delta}SbF_6$ at temperatures of 295 and 10 K.

	$Hg_{3-\delta}AsF_6$ 295 K		$Hg_{3-\delta}AsF_6$ 10 K	$Hg_{3-\delta}SbF_6$ 295 K
	Ref. 1	Ref. 9	Ref. 9	Ref. 8
a (Å)	7.538(4)	7.531	7.443	7.699(31)
c (Å)	12.339(5)	12.395	12.248	12.610(4)
d (Å)	2.64(1)	2.670(5)	2.670(5)	2.64(1)

from the c axis and is not observed below a magnetic field of 4.6 T. In all magnetic field directions, harmonics and combinations of the frequencies were present but are not shown in Fig. 3. It should also be noted that a very low frequency (called α^*) with a value of 48 T was observed at the c direction but is not plotted in Fig. 3. Table II shows the values of the dHvA frequencies and corresponding cross-sectional areas of the Fermi surface measured with the magnetic field along the c axis. Cyclotron masses for γ, δ, and ϵ branches at the c direction are also shown in Table II. No closed Fermi-surface pieces appear to exist since no dHvA frequencies were found in a careful search with magnetic field directions in the (001) plane.

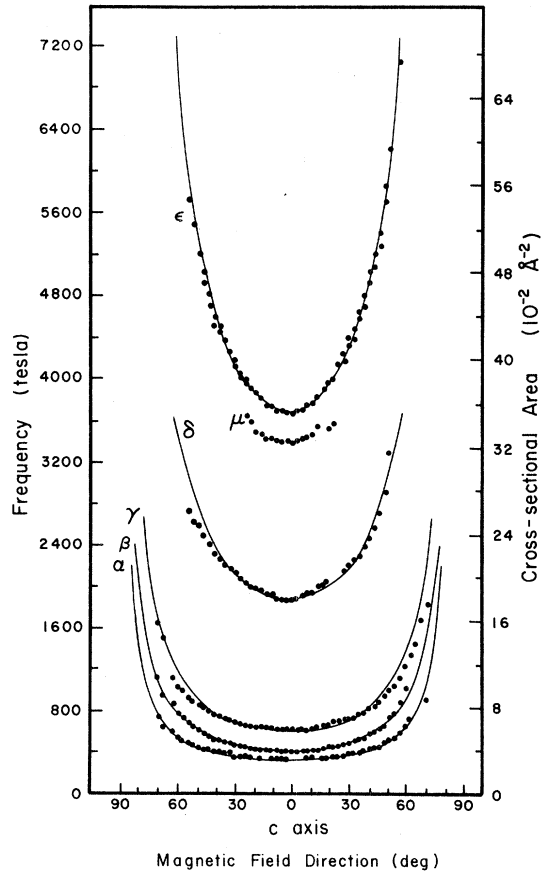

FIG. 3. dHvA frequencies and corresponding cross-sectional areas as a function of magnetic field direction in a plane containing the c axis. Solid lines are for cylindrical Fermi-surface sections.

Since elastic neutron scattering experiments showed that high-temperature, short-range order can be frozen in by rapid cooling of $Hg_{3-\delta}AsF_6$ with no evidence of long-range order, a series of dHvA experiments was done with one sample. The magnetic field direction for these experiments was 20° from the c axis. The sample was immersed in liquid helium from room temperature for the first experiment. Then, the same was warmed to room temperature slowly and cooled to liquid-helium temperature very slowly for the second experiment. The data were taken under the same conditions of magnetic field modulation and magnetic field range in both experiments. The amplitudes of α, β, γ, and ϵ frequencies increased by a factor of 2 in the second experiment while the values of the frequencies remained constant. There was, however, an additional frequency 100 T below the δ frequency in both experiments. The amplitude of the new frequency was nine times larger than the δ frequency for fast cooling of the sample. The reverse was true for slow cooling. The change in amplitude appeared as an overall field-dependent change with no evidence of a modified breakdown field. The Dingle temperature was not measured for different cooling rates. An explanation of this new frequency is not known at the present time although it possibly arises from short-range order of mercury maintained by the rapid quench of the first experiment. Another difference between the two experiments was the appearance of harmonics and combinations of all dHvA frequencies when the sample was cooled slowly.

TABLE II. de Haas–van Alphen frequencies, extremal cross-sectional Fermi-surface areas and cyclotron massed for $Hg_{3-\delta}AsF_6$

Orbit	Experiment			Theory	
	Freq (T)	Area ($Å^{-2}$)	m^*/m_0	Area ($Å^{-2}$)	m^*/m_0
α^*	48	0.0046		0.0046	0.045
α	340	0.0325		0.0285	0.16
β	413	0.0395			
γ	626	0.0598	0.23±.02	0.0599	0.16
δ	1860	0.178	0.27±.08	0.178	0.28
μ	3413	0.326		0.327	0.39
ϵ	3680	0.352	0.33±.01	0.359	0.39

The Dingle temperature was also calculated using the field dependence of the amplitude of the γ frequency. The Dingle plot for the c direction in Fig. 4 has an oscillatory component which is periodic with inverse magnetic field. This oscillatory behavior arises from amplitude modulation (AM) in conjunction with frequency modulation (FM) due to magnetic interaction through modulation of the Bessel function arguments which appear in using the field modulation technique.[10] In this AM-FM effect, the low frequency modulates the amplitude of the high-frequency dHvA wave form causing the oscillatory behavior of the amplitude of the high frequency. The frequency of the modulation is 57.7 T for a direction 20° from the c axis and is on the α^* frequency branch. The Dingle temperature determined from the least-squares fit of the slope of the Dingle plot was found to be

$$1.2\pm0.1K\ .$$

The dHvA effect was observed in four $Hg_{3-\delta}SbF_6$ samples. For each sample sets of frequency branchs were centered at several directions for a 180° angular range of magnetic field. The different sets appeared to arise from different crystallites in the sample and x-ray examination showed that the samples were polycrystalline. One sample contained one major crystal and a few smaller crystals. The set of six dHvA frequency branches from this crystal are shown in Fig. 5. The direction of magnetic field at the branch mini-

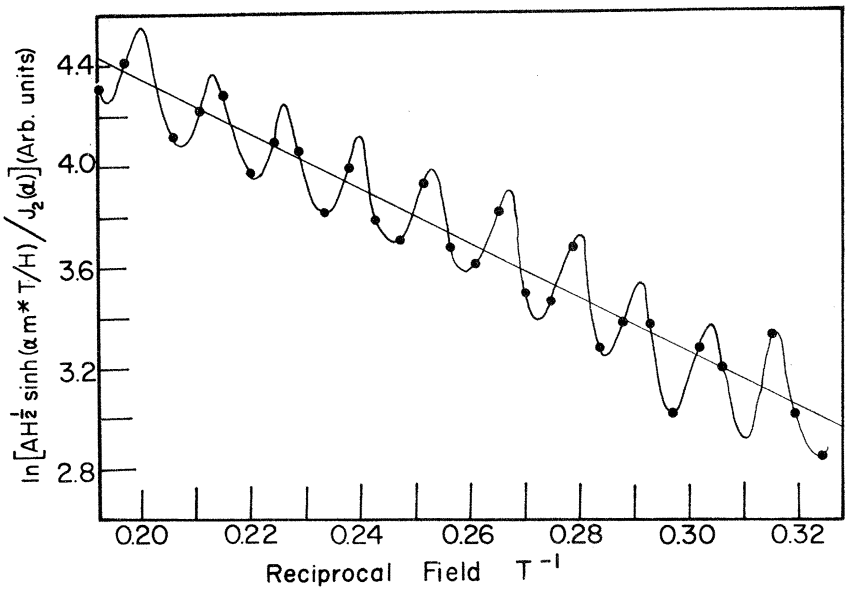

FIG. 4. Log plot used to determine the Dingle temperature for the γ dHvA oscillation with the magnetic field 20° from c axis. The oscillatory behavior of amplitude is due to the AM-FM effect with the frequency 57.7 T.

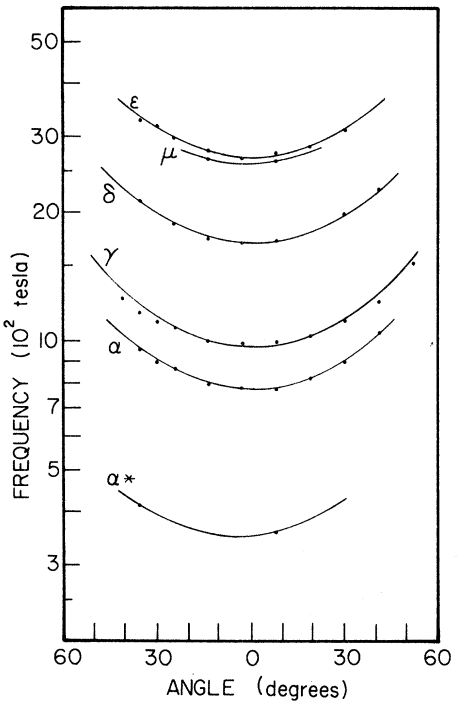

FIG. 5. Semilog plot of the dHvA frequencies as a function of magnetic field direction from the c axis in $Hg_{3-\delta}SbF_6$. Solid lines represent cylindrical fits.

ma is taken to be parallel to the c axis. Values of the six frequencies at this magnetic field direction are listed in Table III. Frequency branches α, γ, δ, and ϵ were observed for magnetic field directions up to 40° away from the c axis. The oscillations for the α^* and μ frequencies were much weaker and existed over a small angular range about the c axis. Cyclotron masses determined from the temperature dependence of the amplitude of the Fourier components of dHvA effect are shown for the c direction in Table III.

The angular dependence of the dHvA frequencies in both compounds suggests pieces of Fermi surface which are cylinders along the c axis. The cross-sectional area of a cylinder varies as $A_0 \sec\theta$, where A_0 is the cross-sectional area perpendicular to the axis of the cylinder and θ is the angle between the magnetic field direction and cylinder axis. The dHvA frequencies in Figs. 3 and 5 follow this $\sec\theta$ dependence closely for values of A_0 and corresponding frequencies F_0 given in Tables II and III, respectively, for the c direction.

IV. FERMI-SURFACE MODEL

The electrical and optical properties of $Hg_{3-\delta}AsF_6$ and $Hg_{3-\delta}SbF_6$ are anisotropic and metallic which suggests that the conduction electrons are localized in the channels containing the mercury chains. There is ionic bonding between the positively charged mercury chains and the hexafluoride anions and metallic bonding between mercury atoms along a chain. The 6s valence electrons of the Hg atoms not required for the ionic bond participate in electrical conduction.

Since the Hg-Hg distance is incommensurate with the tetragonal lattice parameter of the hexafluoride anions, the whole crystal is the smallest unit cell that can be constructed. This makes it impossible to employ the techniques used to calculate the energy band structure of the electrons in other metals. This problem is eliminated by a suggestion[11] that in a first approximation, the positions of the mercury ions along the chains can be ignored so that the electrons move in a cylindrically symmetric uniform potential along the direction of the chains. This potential obeys the same symmetry operations as the lattice of hexafluoride anions.

We start by assuming that chains do not interact which implies that the dispersion relation $\epsilon=\epsilon(\vec{k})$ depends only on the component of $\vec{k}$ along the chain. The Fermi wave vector along the chain k_F

TABLE III. de Haas–van Alphen frequencies, extremal cross-sectional Fermi-surface areas, and cyclotron mass ratios for $Hg_{3-\delta}SbF_6$.

Orbit	Freq (T)	Experiment area (Å^{-2})	m^*/m_0	Theory Area (Å^{-2})	m^*/m_0
α^*	345	0.0330		0.0330	0.12
α	770	0.0735	0.15±.02	0.0738	0.19
γ	975	0.0931		0.0942	0.19
δ	1680	0.160	0.18±.03	0.161	0.27
μ	2580	0.246		0.247	0.34
ϵ	2700	0.258	0.32±.01	0.259	0.34

is determined by filling the lower-energy states with all the available valence electrons. Each mercury atom contributes two valence electrons, but one electron for every $(3-\delta)$ mercury atom is used in bonding the mercury chain to the hexafluoride anions. If the chain's length is L, then the number of mercury atoms along a chain is L/d where d is the mercury-mercury distance. The total number of electrons is

$$N_e=\frac{L}{d}\left[2-\frac{1}{3-\delta}\right]N_c\ , \tag{2}$$

where N_c is the number of chains. The Brillouin zone will be full in the plane perpendicular to the chain because in that plane, the energy is independent of $\vec{k}$. There will not be any occupied states outside the Brillouin zone in the plane perpendicular to the chain where our model consists of a tight-binding band with one orbital on each chain and negligible overlap between orbitals. There will be $2N_c$ filled states for each value of the wave vector along the chain. Equating the number of occupied states to the total number of electrons available gives

$$\left[2k_F\times\frac{L}{2\pi}\right]\times 2N_c=\frac{L}{d}\left[2-\frac{1}{3-\delta}\right]N_c\ , \tag{3}$$

where $L/2\pi$ is the density of states for wave vectors along the chain. Therefore,

$$k_F=\frac{\pi(2.5-\delta)}{a}\ . \tag{4}$$

The Fermi surface for one set of chains consists of two planes perpendicular to the direction of the chains at $+k_F$ and $-k_F$. Since δ is less than 0.5, the first two zones are full and the Fermi vector in the third zone is $(0.5-\delta)\pi/a$.

There are two sets of mutually perpendicular chains in the lattice of the hexafluoride anions. The Fermi surface for the two perpendicular sets of chains in the third Brillouin zone consists of four planes parallel to k_z at

$$k_x,k_y=\pm(0.5-\delta)\pi/a\ .$$

These planes intersect at four lines parallel to k_z. Interchain interaction of any magnitude removes the degeneracies at the lines of interaction and introduces small energy gaps.

It is sufficient to look at the $k_z=0$ cross section since there is no variation of the Fermi surface along k_z in this first approximation. Figure 6 shows this cross section of the Fermi surface and the Brillouin zone of the body-centered tetragonal lattice in the extended zone scheme. The Fermi surface consists of two square cylinders: one electron cylinder centered at Γ and a hole cylinder centered at X. (Of course, the square cross-sections at Γ and Z are the same since Γ is above Z in the k_z direction.) The cross-sectional areas (A) are given by

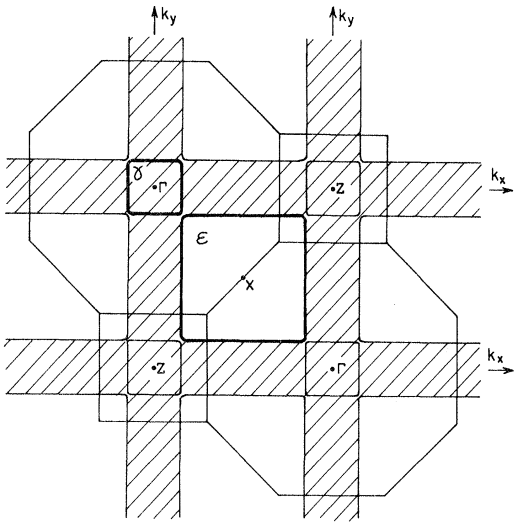

FIG. 6. Cross section of the Fermi surface of $Hg_{3-\delta}AsF_6$ and the body-centered-tetragonal Brillouin zone in the (001) plane in the extended zone scheme. Cross-hatched regions are occupied by electrons. The electron orbit γ and the hole orbit ϵ are outlined.

$$A_e=\left[\frac{\pi}{a}(1-2\delta)\right]^2\ , \tag{5}$$

$$A_h=\left[\frac{\pi}{a}(1+2\delta)\right]^2\ . \tag{6}$$

For $Hg_{3-\delta}AsF_6$, $\delta=0.21$ at a temperature of 10 K according to the parameters shown in Table I. There is excellent agreement between the area of the electron orbit and the measured cross section of the γ cylinder and between the area of the hole orbit and the cross section of the ϵ cylinder as shown in Table II.

The value of δ for $Hg_{3-\delta}SbF_6$ at low temperatures is not known since the crystal structure parameters have not been determined below room temperature. The best agreement between calculated and measured frequencies in Table III is for $\delta=0.135$. This appears to be a reasonable determination of δ at 1.2 K since it would be 0.12 if the mercury distance remained constant from room temperature.

Therefore, it is reasonable to consider that the mercury chains are structureless in a first approximation. This is physically sound at room temperature where there is no ordering between chains. However, below 120 K, the two sets of chains order and form two reciprocal lattices with common reciprocal points at

$$\vec{G}=n(3-\delta,3-\delta,0)\ .$$

As in the case of spin-density waves in chromium,[12] the crystal potential of the mercury chains opens energy gaps in the vicinity of any pair of states on the Fermi surface which are separated by $\vec{q}=\vec{G}$ (AsF_6 lattice)$-\vec{G}$(chains). The smallest nonzero $\vec{q}$ is given by

$$\vec{q}=\frac{2\pi}{a}(\delta,\pm\delta,0)\ ,$$

where the choice of signs corresponds to two possible domains in the crystal. The location of the energy gaps is found by displacing the Fermi surface by $\vec{q}$ and superposing this translated surface on the original, as shown in Fig. 7.

If the energy gap at lines of crossing is very large, the set of orbits shown in Fig. 8 is obtained and the orbits γ and ϵ are not possible. There are four new orbits consisting of two electrons orbits, α^* and $+$, one hole orbit δ, and one open orbit. In $Hg_{3-\delta}AsF_6$ orbit $+$ and open orbits in the (001) plane are not observed.[13] This implies that the energy gaps caused by the extra periodicity associated with the mercury chains are small enough to permit magnetic breakdown across them. Assuming

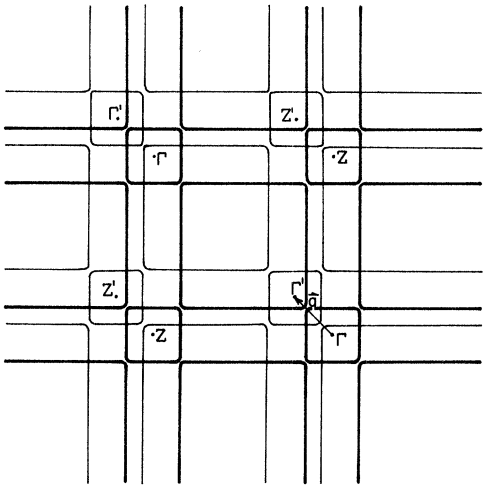

FIG. 7. Fermi surface of $Hg_{3-\delta}AsF_6$ in the (001) plane translated by $\vec{q}$ (light) on to the original Fermi surface (dark).

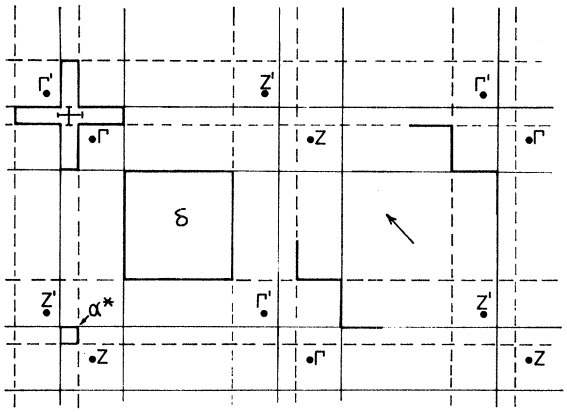

FIG. 8. Closed orbits α^*, δ, and $+$ and an open orbit along the direction of the arrow obtained when the gaps at the intersections of the original Fermi surface (solid lines) and the translated Fermi surface (dashed lines) are large.

that all first-order gaps are the same, we call the corresponding breakdown probability q and determine all the possible orbits if this probability is of the order of 0.5. Then, the α and μ orbits shown in Fig. 9 exist. The orbits predicted for $Hg_{3-\delta}SbF_6$ are shown in Fig. 10. The areas and probabilities of occurrence of possible orbits are given in Table IV.

The electron orbits α, α^*, and γ and the hole orbits δ, ϵ, and μ are observed in $Hg_{3-\delta}AsF_6$ (Table II). Our assignment of the orbit corresponding to frequency α is different from the assignment of Razavi *et al.* The orbit they chose (Fig. 9) is an interferometric orbit[14] which cannot be observed directly in dHvA experiments. The probabilities associated with the orbits that are observed are of

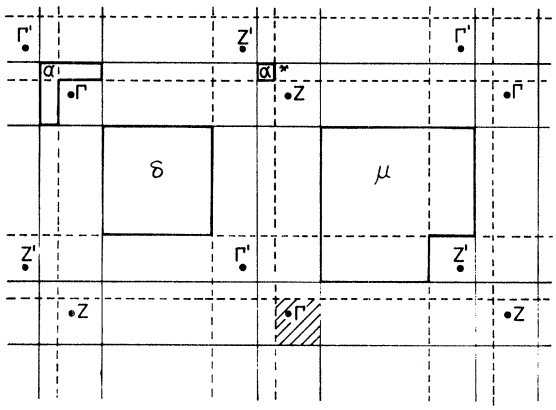

FIG. 9. Orbits α^*, α, δ, and μ for $Hg_{3-\delta}AsF_6$. The contour of the dashed area represents the interferometric orbit assigned previously to the frequency α.

TABLE IV. Areas and probabilities of occurrence of possible orbits associated with our Fermi-surface model of the mercury chain compounds. Ratios of the cross-sectional areas to the area corresponding to the δ orbit are also shown.

Orbit	Area	Probability		Area / Area (δ)
		$Hg_{3-\delta}AsF_6$	$Hg_{3-\delta}SbF_6$	
γ	$\frac{\pi^2}{a^2}(1-2\delta)^2$	q^8	q^8	$(1-2\delta)^2$
ϵ	$\frac{\pi^2}{a^2}(1+2\delta)^2$	q^8	q^8	$(1+2\delta)^2$
μ	$\frac{\pi^2}{a^2}(1+4\delta)$	$(1-q)^2q^8$	$(1-q)^2q^6$	$(1+4\delta)$
α	$\frac{\pi^2}{a^2}(1-4\delta)$	$(1-q)^2q^4$	$(1-q)^2q^6$	$(1-4\delta)$
δ	$\frac{\pi^2}{a^2}$	$(1-q)^2q^4$	$(1-q)^2q^4$	1
α^*	$\frac{\pi^2}{a^2}(1-4\delta)^2$	$(1-q)^2$	$(1-q)^2q^4$	$(1-4\delta)^2$
$2\gamma-\alpha^*$	$\frac{\pi^2}{a^2}(1-8\delta^2)$	$(1-q)^2q^{12}$	$(1-q)^2q^8$	$(1-8\delta^2)$
$2\epsilon-\delta$	$\frac{\pi^2}{a^2}(1+8\delta+8\delta^2)$	$(1-q)^2q^{10}$	$(1-q)^2q^8$	$(1+8\delta+8\delta^2)$
$\gamma+\alpha-\alpha^*$	$\frac{\pi^2}{a^2}(1-12\delta^2)$	$(1-q)^4q^8$	$(1-q)^4q^6$	$(1-12\delta^2)$
$2\epsilon-\delta-\alpha'$	$\frac{\pi^2}{a^2}(1+8\delta+4\delta^2)$	$(1-q)^4q^{10}$	$(1-q)^4q^6$	$(1+8\delta+4\delta^2)$
$\delta-\alpha'$	$\frac{\pi^2}{a^2}(1-4\delta^2)$	$(1-q)^4q^4$	$(1-q)^4q^2$	$(1-4\delta^2)$

low order in $(1-q)$ confirming our suggestion that q is large. Also, the probability of orbit μ, which was shown to disappear below 4.6 T contains the largest power of q. The β orbit observed only in $Hg_{3-\delta}AsF_6$ is not explained readily and could be caused by a complicated breakdown orbit.

Finally, we consider the cyclotron mass of orbits in our model. The energy E is only a function of the component of the wave vector along the chain $k_{||}$, and the areas of the most probable orbits are given by

$$A_\gamma=\left[2k_{||}-\frac{4\pi}{a}\right]^2, \tag{7}$$

$$A_\epsilon=\left[\frac{6\pi}{a}-2k_{||}\right]^2, \tag{8}$$

$$A_\delta=\left[\frac{6\pi}{a}-2k_{||}-\frac{2\pi}{a}\delta\right]^2, \tag{9}$$

$$A_{\alpha^*}=\left[2k_{||}-\frac{4\pi}{a}-\frac{2\pi}{a}\delta\right]^2, \tag{10}$$

$$A_\alpha=A_\gamma-\frac{4\pi^2}{a^2}\delta^2, \tag{11}$$

$$A_\mu=A_\epsilon-\frac{4\pi^2}{a^2}\delta^2, \tag{12}$$

so that, for orbits γ, ϵ, δ, and α^*, we have

$$m^*_\gamma, m^*_{\alpha^*}>0, \quad m^*_\delta, m^*_\epsilon<0, \tag{13}$$

and

$$|m^*|=\frac{2\hbar^2}{\pi}\sqrt{A}\,k'_{||}, \tag{14}$$

where

$$k'_{||}=\frac{dk_{||}}{dE}.$$

Assuming a strictly free electron dispersion relation along the chain,

$$|m^*|=\frac{2m}{\pi}\left[\frac{A}{k^2_{||}}\right]^{1/2} \tag{15}$$

where m is the free-electron mass.

There are two pairs of orbits with the same mass:

$$m^*_\alpha=m^*_\gamma \text{ and } m^*_\mu=m^*_\epsilon.$$

With $\delta=0.210$ and $a=7.442$ Å for $Hg_{3-\delta}AsF_6$ and $\delta=0.135$ and $a=7.843$ Å for $Hg_{3-\delta}SbF_6$, we obtain the cyclotron masses in Tables II and III. They are in reasonable agreement with the experimental values.

V. DISCUSSION

The dHvA frequencies of similar orbits are quite different in the two compounds. The smallest orbit has a frequency of 48 T in $Hg_{3-\delta}AsF_6$ and 345 T in $Hg_{3-\delta}SbF_6$. The largest frequency is 3680 in $Hg_{3-\delta}AsF_6$ and 2700 T in $Hg_{3-\delta}SbF_6$. The difference in the incommensurability parameter δ causes the large differences in the areas of the orbits but does not change the topology of the Fermi surface except for some of the more complicated orbits.

Ratios of orbit areas to the area of the δ orbit are simple functions of the parameter δ. Predicted frequency ratios for values of δ between 0.10 and 0.23 are shown in Fig. 11. This change with δ is observed and is shown for the two compounds at zero pressure and for $Hg_{3-\delta}AsF_6$ at a pressure of 4 kbar.[15]

In our model, the α and δ frequencies result from ordering within and between mercury chains while the γ and ϵ frequencies depend only on the host lattice. However, the degree of ordering depends on the rate of cooling.[9] The α and δ oscillations should therefore be reduced relative to the γ and ϵ oscillations for rapid cooling. Decreased amplitude of the α and δ oscillations has been observed in our experiments with different cooling rates. The change in amplitude gives an indication of the amount of ordering for different cooling conditions.

In our model a two-dimensional Fermi surface results from coupled one-dimensional energy bands. This coupling should cause an undulation of the cylinders with the periodicity of the lattice along the c direction. This small deviation from a straight cylinder gives a c axis electron velocity component and electrical conductivity along the c axis. It should also be evident in deviations from the cylindrical fit of the dHvA data. Indeed, there are small deviations from the cylindrical fits in Figs. 3 and 5, but they are small and depend too much on the cylindrical fit to provide information about the Fermi-surface undulations.

The values of all the dHvA frequencies in our model depend only on the tetragonal lattice parameter a and the mercury-mercury distance d. Therefore, by applying hydrostatic pressure to these compounds, the dHvA frequencies should change significantly. We have observed such changes for $Hg_{3-\delta}AsF_6$ between 0 and 5 kbar (Ref. 15) and accounted for these changes in terms of a 0.7% contraction of the hexafluoride anion lattice while the mercury-mercury distance remained constant.

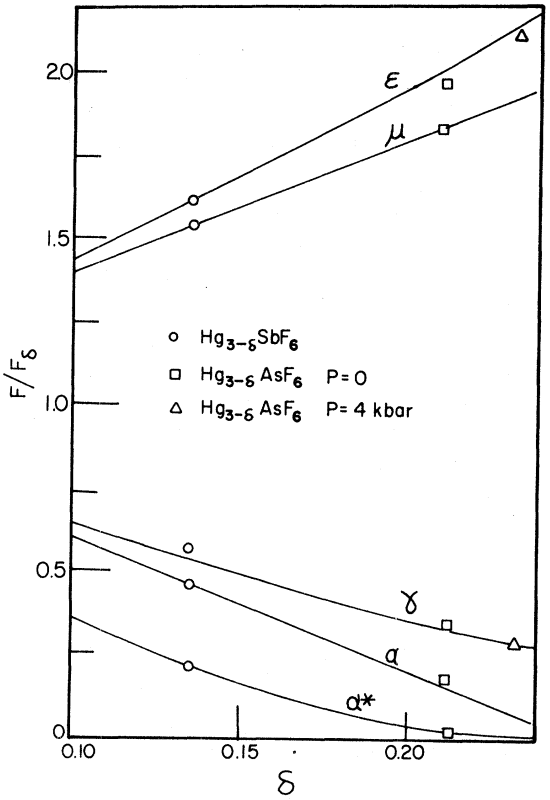

FIG. 11. Theoretical ratios of the α^*, α, γ, μ, and ϵ frequencies to the δ frequency as a function of the incommensurability parameter δ. Experimental data are shown for $Hg_{3-\delta}SbF_6$ and $Hg_{3-\delta}AsF_6$.

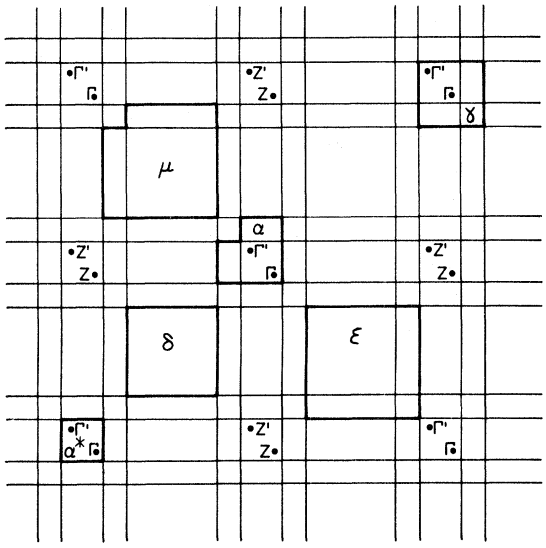

FIG. 10. Orbits α^*, α, γ, δ, μ, and ϵ for $Hg_{3-\delta}SbF_6$.

Other properties related to the Fermi surface, especially transport properties, should be very easy to calculate within the framework of this model because the Fermi-surface cylinders ideally have perfectly flat faces normal to the x and y direction so that the electron velocity $\vec{v}_k = \hbar^{-1}\vec{\nabla}_{\vec{k}}\epsilon$ is along $\hat{x}$ and $\hat{y}$. Of course, at the corners of the square cross section the electron velocity has to turn by 90° over an interval that depends on how much the cross section differs from a perfect square.

Also, although we have assumed that the Fermi-surface gaps created by the translation of the Fermi surface by $\vec{q}$ because of the ordering of the mercury chains below 120 K are all equal, it is likely that this is so and it would be of interest to estimate the size of these gaps experimentally.

VI. CONCLUSIONS

There are six dHvA frequency branches for $Hg_{3-\delta}AsF_6$ and $Hg_{3-\delta}SbF_6$. They indicate that the Fermi surface consists of straight or nearly-straight Fermi-surface cylinders with axes along the c axis. The Fermi surface of these compounds is formed by filling one-dimensional states along the a and b directions of the tetragonal lattice and having coupling between the one-dimensional states. This forms a two-dimensional Fermi surface. The low-temperature structure of the mercury chains, which is incommensurate with respect to the tetragonal lattice, provides a perturbing potential. The Fermi surface is displaced by a vector equal to the difference between wave vectors of the two periodicities. Energy gaps exist at intersections of the displaced and nondisplaced Fermi surface.

ACKNOWLEDGMENTS

The Fermi-surface model was developed through discussions with A. J. Berlinsky. Samples of both compounds were prepared by D. Chartier. Useful discussion with R. J. Gillespie is also acknowledged. The research was supported by a grant from the Natural Sciences and Engineering Research Council of Canada.

[1]I. D. Brown, B. D. Cutforth, C. G. Davies, R. J. Gillespie, P. R. Ireland, and J. E. Vekris, Can. J. Chem. 52, 791 (1974).
[2]B. D. Cutforth, W. R. Datars, A. van Schyndel, and R. J. Gillespie, Solid State Commun. 21, 377 (1977).
[3]C. K. Chiang, R. Spal, A. M. Denenstein, A. J. Heeger, N. D. Miro, and A. G. MacDiarmid, Solid State Commun. 22, 293 (1977).
[4]E. S. Koteles, W. R. Datars, B. D. Cutforth, and R. J. Gillespie, Solid State Commun. 20, 1129 (1976).
[5]D. L. Peebles, C. K. Chiang, M. J. Cohen, A. J. Heeger, N. D. Miro, and A. G. MacDiarmid, Phys. Rev. B 15, 4607 (1977).
[6]F. S. Razavi, W. R. Datars, D. Chartier, and R. J. Gillespie, Phys. Rev. Lett. 42, 1182 (1979).
[7]E. Batalla, W. R. Datars, D. Chartier, and R. J. Gillespie, Solid State Commun. 38, 1203 (1981).
[8]B. D. Cutforth, Ph.D thesis (McMaster University, 1975) (unpublished).
[9]J. P. Pouget, G. Shirane, J. M. Hastings, A. J. Heeger, N. D. Miro, and A. G. MacDiarmid, Phys. Rev. B 18, 3645 (1978).
[10]H. Alles and D. H. Lowndes, Phys. Rev. B 8, 5462 (1973).
[11]A. J. Berlinsky (private communication).
[12]W. M. Lomer, *Proceedings of the International Conference on Magnetism, Nottingham, England, 1964* (The Institute of Physics and the Physical Society, London, England, 1965), p. 127.
[13]R. J. Dinser, W. R. Datars, D. Chartier, and R. J. Gillespie, Solid State Commun. 32, 1041 (1979).
[14]R. W. Stark and C. B. Friedberg, Phys. Rev. Lett. 26, 556 (1971).
[15]E. Batalla, W. R. Datars, D. Chartier, and R. J. Gillespie, Solid State Commun. 40, 711(1981).